Urban Forestry & Urban Greening 104 (2025) 128624

Contents lists available at ScienceDirect

Urban Forestry & Urban Greening

journal homepage: www.elsevier.com/locate/ufug

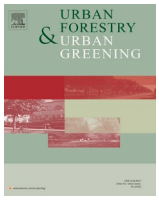

Original article

Impacts of 2D/3D building morphology on vegetation greening trends in Hong Kong: An urban-rural contrast perspective

Yu Liu [a,b], Qihao Weng [a,b,c,*]

[a] JC STEM Lab of Earth Observations, Department of Land Surveying and Geo-Informatics, The Hong Kong Polytechnic University, Hung Hom, Hong Kong
[b] Research Centre for Artificial Intelligence in Geomatics, The Hong Kong Polytechnic University, Hung Hom, Hong Kong
[c] Research Institute for Land and Space, The Hong Kong Polytechnic University, Hung Hom, Hong Kong

ARTICLE INFO

Keywords:
Vegetation greening
2D/3D building morphology
Urban-rural difference
Boosted regression tree
Sustainable development goals
Hong Kong

ABSTRACT

Building morphology profoundly impacts the microclimate, potentially affecting vegetation greening. However, the effects of 2D/3D building morphology on vegetation greening, especially the urban-rural disparities, remains understudied. In this study, we examined the effects of building morphology on vegetation greening in urban and rural areas in Hong Kong by employing a machine learning model. Vegetation greening trends were derived using the Enhanced Vegetation Index (EVI) through the Theil-Sen median method and the Mann-Kendall (MK) test. Results indicated a prevalent greening from 2010 to 2020, with a slope of 0.0024, and more significant in rural. Statistically significant but low correlation existed between building morphology and vegetation greening. Their relationship exhibited notable urban-rural differences and non-monotonic nonlinearity, with 3D indexes showing a stronger impact than 2D indexes. Specifically, sky view factor (SVF) dominated in urban areas, contributing 23.60 %, while landscape shape index (LSI) was the key contributor in rural, accounting for 27.30 %. SVF, and mean building height (MBH) transitioned from negative to positive effects, whereas landscape patch index (LPI) and edge density (ED) shifted from positive to negative effects, each with distinct "turning points" in urban and rural. LSI's impact showed a negative-positive-negative shift in urban and a negative-positive shift in rural. Building volume density (BVD) presented a positive to negative shift in urban and negative to positive shift in rural. The identified complicated relationship deepens our understanding of the drivers of vegetation greening in the built environment, informing the optimal building morphology threshold for efficient greening effect toward sustainable development.

1. Introduction

Vegetation is a crucial component of the terrestrial ecosystem that plays an indispensable role in soil and water conservation, moisture retention, and the cycles of carbon and energy (Ballantyne et al., 2017; Haberl et al., 2007). Globally, vegetation greenness has undergone complex changes over the past few decades due to the combined effects of climate change and human activities (Li et al., 2024; Myneni et al., 1997; Pan et al., 2018; Zhu et al., 2016). Many studies have highlighted the critical role of vegetation greening in mitigating climate change, enhancing ecosystem services, and improving human well-being (Baniya et al., 2019; Zeng et al., 2017). Therefore, comprehending the trends and drivers of vegetation greening is crucial to achieving Sustainable Development Goal 11.

Differing from natural landscapes, vegetation in built environments is affected by more complex and multidimensional factors (Liu et al., 2023). Although extensive efforts have been made to understand the sophisticated response of vegetation greening in the built environment to various natural and anthropogenic drivers (Fan et al., 2023; Li et al., 2020), how building morphology affects vegetation greening trends is still not well understood. Building morphology could potentially influence vegetation greening trends by altering the growth environment. Numerous studies have demonstrated that the building morphology affects microclimate (Allen-Dumas et al., 2020; Zhang et al., 2022), including the temperature conditions (Azhdari et al., 2018; Han et al., 2023; Li and Hu, 2022), wind direction and speed (He et al., 2022; Zahid Iqbal and Chan, 2016), distribution of photosynthetically active radiation and shadows (Tan and Ismail, 2015; Wang et al., 2024), and

* Corresponding author at: JC STEM Lab of Earth Observations, Department of Land Surveying and Geo-Informatics, The Hong Kong Polytechnic University, Hung Hom, Hong Kong.
E-mail address: qihao.weng@polyu.edu.hk (Q. Weng).

https://doi.org/10.1016/j.ufug.2024.128624
Received 12 July 2024; Received in revised form 19 November 2024; Accepted 26 November 2024
Available online 29 November 2024

humidity levels (Cao et al., 2021; Kamal et al., 2021). These factors are crucial contributors to vegetation greening, impacting transpiration, photosynthesis, and metabolic rates (Chang et al., 2021; Rawson et al., 1977; Serbin et al., 2015). Therefore, quantifying how building morphology affects vegetation greening is vital for understanding its mechanisms. Previous studies have only focused on the relationship between vegetation greening and two-dimensional (2D) building morphology (Zhang et al., 2022; Zhao et al., 2016; Zhou et al., 2023). For instance, Li et al. (2024) assessed the nonlinear effects of built-up land patterns on vegetation growth in Kunming city from a horizontal perspective. Three-dimensional (3D) building morphology plays a significant role in altering local climate conditions (Salvati et al., 2019; Yang et al., 2023), an aspect that has been largely overlooked in existing literature. Thus, simultaneously discussing the impact of 2D/3D building morphology on vegetation greening trends within built environments is necessary.

Recent studies indicate that vegetation greening trends exhibit significant spatial heterogeneity across the urban-rural gradient (Ji et al., 2023; Yao, 2024). For example, Li et al. (2023) found that the urban-rural gradient in vegetation greening is vividly featured by a 'V-shape', with different influencing factors in urban and rural areas. Land surface properties, climate conditions, vegetation types, vegetation composition and configuration, and anthropogenic activities vary between urban and rural areas (Jia et al., 2021; X. Wang et al., 2024). These disparities may lead to different influencing characteristics of 2D/3D building morphology on vegetation greening, which requires differentiated management and planning strategies for urban and rural areas. Consequently, it is imperative to figure out the urban-rural differences of the relationship between 2D/3D building morphology and vegetation greening trends to provide a reference for differentiated optimizing of building morphology to enhance the greening in urban and rural areas.

Hence, the overall aim of this study is to introduce the boosted regression tree (BRT) model to investigate the relative contributions and marginal effect of 2D/3D building morphology on vegetation greening trends from 2010 to 2020 in Hong Kong and to analyze differences between urban and rural areas. Specific objectives of this study are: 1) to explore the spatial-temporal characteristics and urban-rural differences of vegetation greening trends in Hong Kong from 2010 to 2020; 2) to assess the relative contributions and marginal effect of 2D/3D building morphology on vegetation greening; and 3) to compare the different impacts of 2D/3D building morphology on vegetation greening in urban and rural areas. Insights from this study could deepen our understanding of the factors influencing vegetation greening in built environment.

2. Study area and data

2.1. Study area

Hong Kong is located along the southern coast of China (22°08′-22°35′, 113°49′-114°31′) and spans an area of 1106 km^2 (Fig. 1). It has a typical subtropical climate characterized by mild winters and hot, rainy, and muggy summers. Over 80 % of its total area is covered by hills, leaving just 20 % for the accommodation of more than seven million residents. As one of the most developed cities in China, Hong Kong has undergone remarkable urbanization. Limited land availability has led to densely packed high-rise buildings and complex building morphology, dramatically affecting the local climate in Hong Kong. Furthermore, as Hong Kong has already entered the later stages of urbanization, extensive urban expansion has been almost non-existent since 2010. Instead, Hong Kong retains many unchanged buildings with relatively stable green spaces. Therefore, Hong Kong was considered an ideal laboratory for researching the impacts of 2D/3D building morphology on vegetation greening trends, which will provide valuable insights for other similar and developing high-density cities.

2.2. Data and pre-processing

The 250 × 250 m grid was selected as the most relevant scale for urban microclimate and vegetation greening studies (Li et al., 2024).

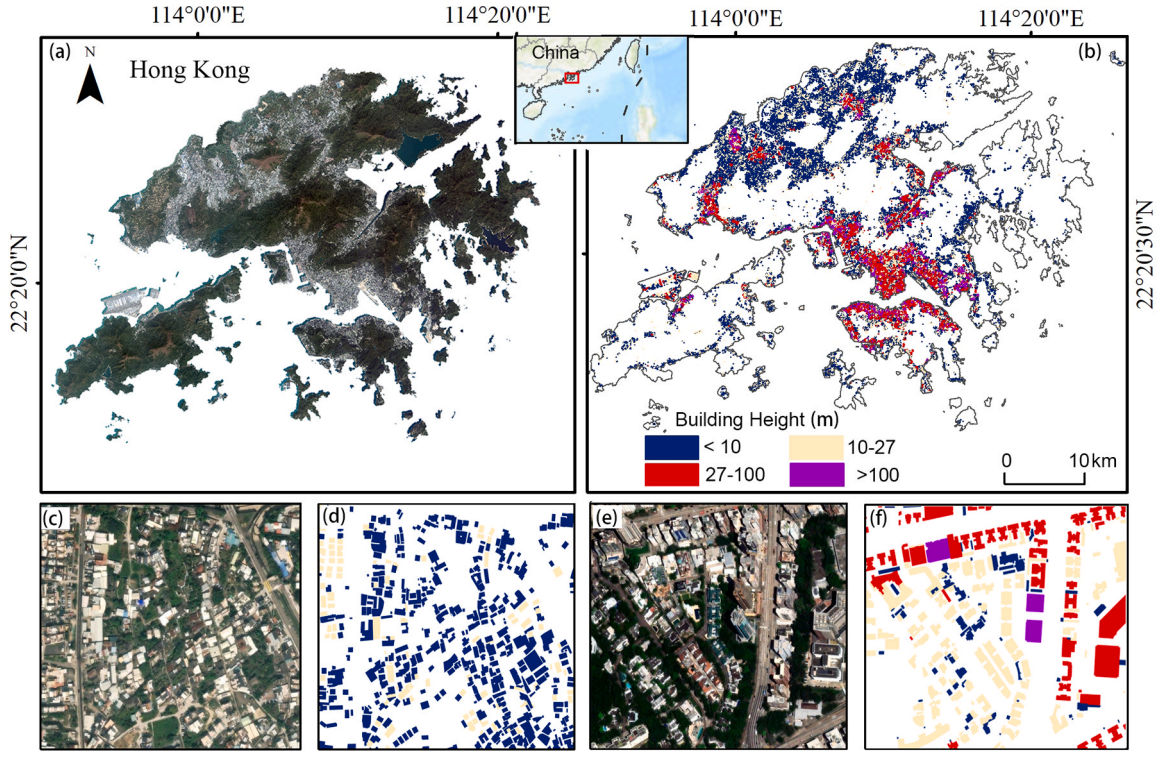

Fig. 1. Hong Kong as seen from GaoFen-1 high-resolution image (a), distribution of buildings with heights (b), zoomed-in high-resolution image (c, e), and corresponding building height data (d, f). Data sources: GaoFen-1 high-resolution image acquired on 22 Feb 2020 from https://www.cresda.com/.

This study utilized the 250 m and 16-day composite Enhanced Vegetation Index (EVI) from the Terra Moderate Resolution Imaging Spectroradiometer (MODIS) Vegetation Index (MOD13Q1) version 6 product to derive the vegetation greening trends in Hong Kong from 2010 to 2020. The EVI index has been proven more suitable for monitoring vegetation variability, as it partially eliminates the effect of clouds, aerosols, and saturation problems (Huete et al., 2002). We calculated the annual averaged composite EVI from the monthly maximum composite during the growing seasons (from June 1st to September 30th every year) (Ru et al., 2018) on the Google Earth Engine (GEE) platform. Pixels with low confidence were removed based on the quality assessment layer.

Building footprint data, digital surface model (DSM), and digital terrain model (DTM) data from 2010 and 2020 were employed to map the building height, which was obtained from Hong Kong Common Spatial Data Infrastructure (CSDI) (https://www.csdi.gov.hk/zh-hk). DSM and DTM data were generated from the LiDAR data in 2010 and 2020. The normalized DSM (nDSM) layer, representing the height of above-ground features, was created by subtracting the DTM from the DSM. Then, building height data for 2010 and 2020 were generated by overlaying building footprint and nDSM data using zonal statistics analysis.

The Global Urban Boundary (GUB) dataset, derived from the high-resolution (30 m) Global Artificial Impervious Area mapping product (GAIA) (Gong et al., 2020), was utilized to define urban and rural areas in 2010. To match the spatial resolution of the EVI data, all the aforementioned data were resampled to 250 m.

3. Methodology

3.1. Overall workflow

This study sought to explore the impacts of 2D/3D building morphology on vegetation greening trends in both urban and rural areas. The overall workflow of this study is illustrated in Fig. 2. First, we derived vegetation greening trends from 2010 to 2020. Subsequently, areas with unchanged building heights from 2010 to 2020 were identified to mitigate the impact of coverage variations on greenness changes. Next, we calculated the 2D/3D building morphology indexes in 2020 to represent the static building morphology indexes. Finally, we analyzed the correlation and nonlinear effects of 2D/3D building morphology on vegetation greening in urban and rural areas.

3.2. Detection of vegetation greening trends from 2010 to 2020

In this study, the vegetation greening trends were analyzed by using the Theil-Sen median method and the annual composite EVI dataset from 2010 to 2020. The Theil-Sen median method, a robust nonparametric statistical approach, is widely used to analyze geographical phenomena over long-term series. The equation of the Theil-Sen median method is as follows:

$$EVI_{slope} = Median\left(\frac{EVI_b - EVI_a}{b-a}\right), 2010 < b < a < 2020 \quad (1)$$

where EVI_{slope} is the Theil-Sen median, EVI_b and EVI_a represent the average growing season EVI values of the years a and b. When EVI_{slope} is greater than zero, it indicates a vegetation greening trend. When it is lower than zero, it indicates a vegetation browning trend.

The Mann–Kendall (MK) test was utilized to assess the significance of vegetation greening and browning trends. The MK test, a nonparametric statistical method, is widely used to analyze trends in time series data. The MK test does not require the data to follow a specific distribution and is robust against outliers. The formula for the MK test is as follows:

$$S = \sum_{a=1}^{n-1} \sum_{b=a+1}^{n} \mathrm{sgn}(EVI_b - EVI_a) \quad (2)$$

$$\mathrm{sgn}(EVI_b - EVI_a) = \begin{cases} +1, & EVI_b - EVI_a > 0 \\ 0, & EVI_b - EVI_a = 0 \\ -1, & EVI_b - EVI_a < 0 \end{cases} \quad (3)$$

$$Var(S) = \frac{n(n-1)(2n+5)}{18} = \sigma^2 \quad (4)$$

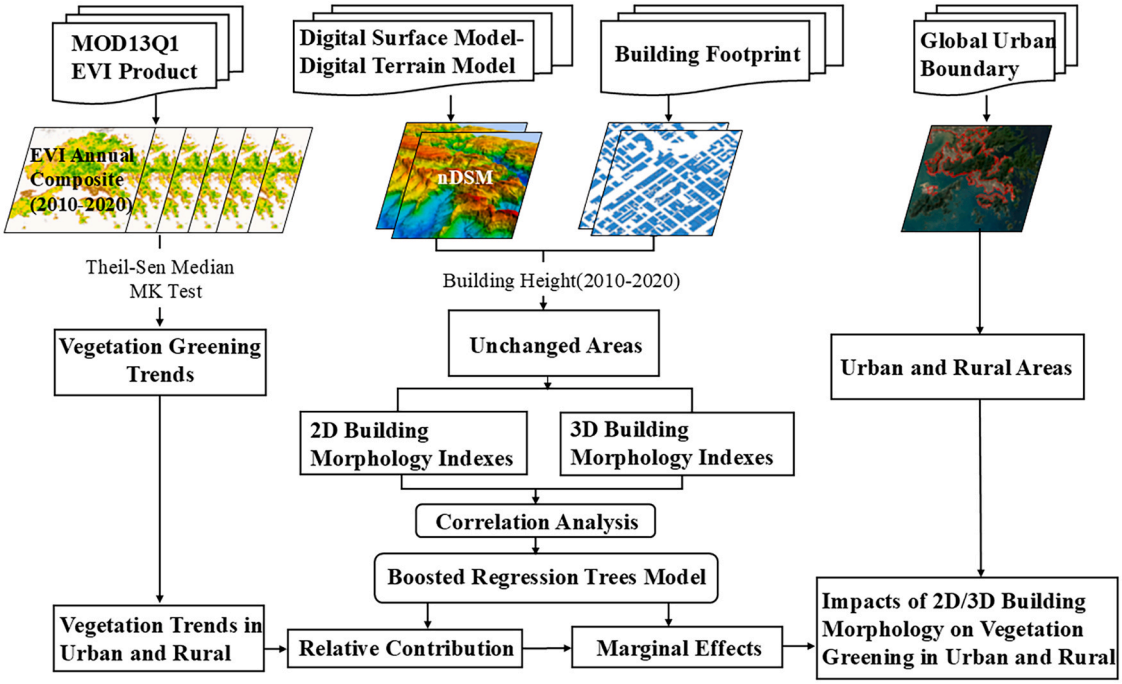

Fig. 2. The overall workflow of this study.

$$Z = \begin{cases} \dfrac{S-1}{\sqrt{Var(S)}}, S > 0 \\ 0, \quad S = 0 \\ \dfrac{S-1}{\sqrt{Var(S)}}, \quad S < 0 \end{cases} \tag{5}$$

where n is the length of the EVI time series, σ is the standard deviation, and $|Z| > 1.96$ was considered to indicate a significant change at the 0.05 significance level.

3.3. Delineation of urban and rural areas

We adopted a binary method to define the urban and rural areas. Urban and rural areas were delineated based on the Global Urban Boundary (GUB) dataset (Li et al., 2020). The GUB dataset, derived from the 30 m global artificial impervious area (GAIA) data, was mapped by using the Landsat times series images and machine learning model. The overall accuracy of the GAIA data was higher than 90 %, and GUB data showed a good agreement with the map derived from other remote sensing data and human interpretation. It can effectively outline the urban extent of cities when evaluated against high-resolution images from Google Earth. Unlike other products (e.g., NTL-derived urban extent), the GUB dataset excels in delineating detailed urban boundaries, particularly around urban fringe areas. Thus, it is widely applied in urban-rural difference-related studies (Ji et al., 2023). In this study, the urban areas were defined by pixels within the urban boundary obtained from the GUB data. The rural areas were defined as pixels outside these urban boundaries.

3.4. Calculation of 2D/3D building morphology indexes

Numerous metrics have been employed to quantify building morphology. We selected four indexes of 2D building morphology and four indexes of 3D building morphology to represent the building morphology in the built environment. The 2D building morphology indexes included the largest patch index (LPI) (Yuan et al., 2021), building coverage ratio (BCR) (Zeng et al., 2022), landscape shape index(LSI) (Liu et al., 2017), and edge density (ED) (Zhou et al., 2011). 3D morphology indicators included building volume density (BVD), sky view factor (SVF) (Daramola and Balogun, 2019), mean building height (MBH) (Alexander, 2021), and floor area ratio (FAR) (Chen et al., 2022). These indexes were chosen for their ability to: (1) describe building morphology from different aspects, (2) serve as common and representative measures, and (3) demonstrate minimal redundancy (Li and Wu, 2004; Li et al., 2012). For the 2D indicators, BCR, a widely used 2D index, represents building density and has been shown to directly impact local climate (Rhee et al., 2014; Zhang et al., 2022). LPI, LSI, and ED were frequently chosen to measure connectivity, complexity, and fragmentation of landscape. The degree of LPI, LSI, and ED of buildings are associated closely with thermal conditions and air circulation (Han et al., 2023). For the 3D indicators, SVF is an essential factor in 3D building related analysis and can exert strong influence on illumination, wind, and heat (Li and Hu, 2022). BVD, MBH, and FAR are also widely adopted in existing research to reflect different distribution features of building volume and height from various perspectives. They have been identified as affecting factors of air and land surface temperature, wind velocity and speed, and relative humidity (Cao et al., 2021). The abbreviations and definitions of the selected building morphology indicators are listed in Table 1. Maps illustrating the 2D/3D building morphology and its changes between 2010 and 2020 can be found in the Appendix (Figure A1-A8).

Table 1
2D/3D building morphology metrics used in this study.

Dimension	Metrics	Abbreviations	Formula	Description
2D	Largest patch index	LPI	$LPI = \frac{\max(A_i)}{S_g} \times 100$	Measures the percentage of the total grid area comprised of the largest patch
	Building coverage ratio	BCR	$BCR = \frac{1}{S_g}\sum_{i=1}^{n} A_i$	Measures the ratio between the total area of buildings within a grid and the total grid area
	Landscape shape index	LSI	$LSI = \frac{\sum_{i=1}^{n} P_i}{0.25 \times \sqrt{\sum_{i=1}^{n} A_i}}$	Measures the degree of landscape shape complexity
	Edge density	ED	$ED = \frac{\sum_{i=1}^{n} P_i}{S_g}$	Measures the total lengths of all building patch edges within a grid
3D	Building volume density	BVD	$BVD = \frac{1}{S_g}\sum_{i=1}^{n} V_i$	Measures the ratio between the total volume of the buildings in a grid and the total grid area
	Sky view factor	SVF	$SVF = 2\pi\left[1 - \frac{\sum_{i=1}^{n}\sin\alpha_j}{n}\right]$	α is the vertical angle of the horizon in the direction j
	Mean building height	MBH	$MBH = \frac{\sum_{i=1}^{n} H_i}{n}$	Measures the mean height of the buildings in a grid
	Floor area ratio	FAR	$FAR = \frac{\sum_{i}^{n}(c \times A_i)}{S_g}$	Measures the total building floor area compared to the land area it occupies in a grid

Note: n is the number of buildings within a grid; Sg is the total area of the grid; Ai, Pi, Vi, Hi, c are the area, perimeter, volume, height, and the number of floors for the ith building, respectively; θ is the wind direction angle.

3.5. Analysis of the impacts of 2D/3D building morphology on vegetation greening trends

Spearman and Pearson correlation coefficients were computed to measure the correlations between 2D/3D building morphology indexes and vegetation greening trends. The Pearson correlation coefficient was primarily used to measure the strength of a linear relationship between two variables (Pearson, 1908), while Spearman correlation coefficient was used to assess the monotonic relationship between two variables,

regardless of whether the relationship is linear or nonlinear (Spearman, 1987). The boosted regression tree (BRT) model was utilized to investigate the nonlinear impacts of 2D/3D building morphology on vegetation greening trends in Hong Kong. The BRT model, a machine learning method, combines the strengths of regression tree models and boosting models to improve stability and prediction precision (De'ath, 2007). Unlike traditional linear regression, BRT uses recursive binary splitting to handle predictor interactions and builds numerous small regression trees to capture complex and nonlinear relationships expressed by relative contribution and marginal effect curve. Relative contribution provides the importance and contribution of 2D/3D building morphology to vegetation greening. Marginal effect presents how this influence changes with variations in the magnitude of 2D/3D building morphology. The relative influence value presented in the marginal effect curve equal to 0 indicates no influence, less than 0 indicates a negative effect, and greater than 0 indicates a positive effect. BRT's advantages include handling flexible data types without considering variable interactions and offering intuitive insights into variable contributions and response curves (Pouteau et al., 2011). Consequently, BRT has been widely used in urban ecosystem studies (Han et al., 2022; Hu et al., 2020). To avoid interference from changes in building and vegetation coverage when analyzing the impact of 2D/3D building morphology on vegetation greening, the unchanged areas that exhibited no changes in both building footprint and height from 2010 to 2020 were identified using spatial analysis tools. The dependent variables are the vegetation greening trends in each unchanged 250 m grid cell, with no changes in building footprint and height from 2010 to 2020. The independent variables are eight static 2D/3D building morphology indexes identified within each unchanged 250 m grid cell. After much debugging, the final parameters used to design the BRT were 0.005 (learning rate), 0.5 (bag fraction), and 5 (tree complexity). Moreover, 50 % of the data was drawn for training, and 10 cross-validations were conducted.

4. Results

4.1. Spatial-temporal patterns of vegetation greening trends, 2010–2020

Overall, we observed a prevalent trend of vegetation greening in Hong Kong from 2010 to 2020, indicated by a greening slope of 0.0024, with approximately 69.10 % of the areas exhibiting the greening phenomenon (Fig. 3). In built-up areas, the overall EVI slope was 0.0015.

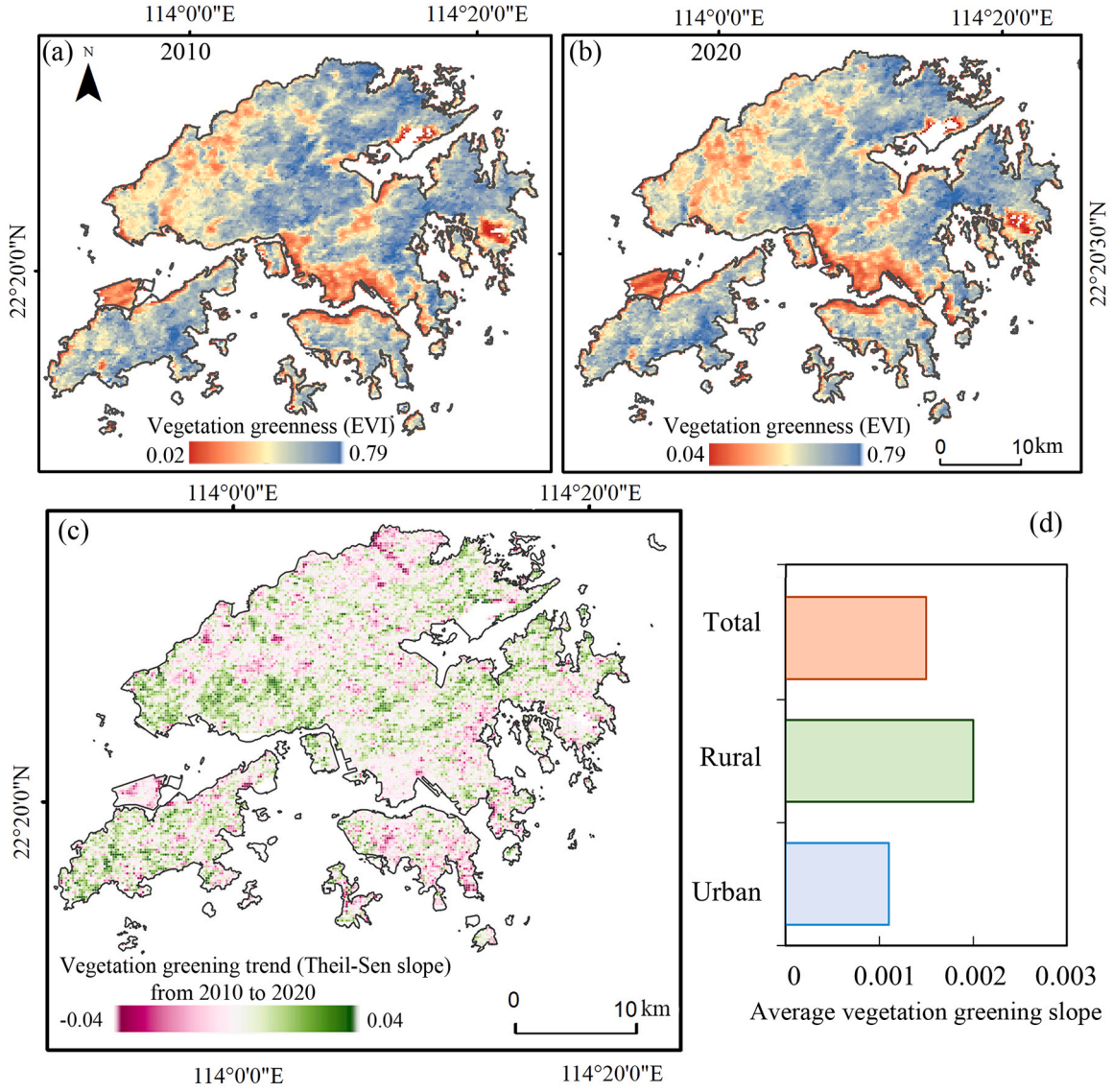

Fig. 3. Spatial pattern of vegetation greenness in 2010 (a) and 2020 (b), vegetation greening trend from 2010 to 2020 (c), and average vegetation greening slope in urban and rural areas (d).

Significant greening and significant browning accounted for 11.89 % and 4.30 % of the areas, respectively, with averaged slopes of 0.0078 and −0.0083, while not significant greening and not significant browning accounted for 52.23 % and 31.42 % of the areas, respectively, with average slopes of 0.0034 and −0.0027 (Table 2). The average vegetation change slope was 0.0011 in urban areas and 0.0020 in rural areas, indicating a more pronounced vegetation greening trend compared to urban areas.

Noticeable disparities were observed in the average slopes and percentages of vegetation greening and browning between urban and rural areas (Table 3). In urban areas, greening accounted for 62.71 % with an average slope of 0.0035, and browning comprised 37.22 % with an average slope of −0.0031. Rural areas showed a higher proportion of greening at 65.38 % and a steeper average slope of 0.0050, compared to urban areas. Conversely, rural areas had a smaller proportion of browning at 34.60 %, but with a slightly steeper average slope of −0.0037.

4.2. Correlation between 2D/3D building morphology and vegetation greening trends

Both Pearson and Spearman correlation analysis results confirmed a low, yet statistically significant, correlation between 2D/3D building morphology and vegetation greening trends (correlation coefficient ranged from −0.21–0.17) (Table 4). The results of the Pearson and Spearman correlation analyses were quite similar, with slight differences, and the positive and negative direction of the correlation was consistent. Furthermore, the correlation between 2D building morphology and vegetation greening was stronger than that with 3D building morphology, which was evidenced by the average absolute value of the Pearson and Spearman correlation coefficient. Among various factors, the SVF demonstrated a positive correlation with vegetation greening trends, with a correlation coefficient of 0.17 and 0.15, respectively. The BCR, LPI, LSI, ED, BVD, MBH, and FAR all exhibited negative correlations with vegetation greening.

4.3. Impacts of 2D/3D building morphology on vegetation greening trends

4.3.1. Relative contribution of 2D/3D building morphology on vegetation greening trends

The relative contribution of 2D/3D building morphology on vegetation greening trends varied significantly between urban and rural areas (Fig. 4). In urban areas, the SVF contributed most significantly to vegetation greening, accounting for 23.60 % of the independent effects. This was followed by LPI at 20.10 %, MBH at 19.00 %, BVD at 12.00 %, LSI at 11.50 %, and ED at 13.30 %. The relative contributions of FAR and BCR to vegetation greening were minimal. In rural areas, LSI was the predominant index affecting vegetation greening, with a relative contribution of 27.30 %, followed by SVF (22.80 %), and MBH (17.50 %). The contributions of ED, LPI, BVD, FAR, and BCR were lower.

3D building morphology indexes contributed more to vegetation greening trends than 2D indexes (Fig. 4). This phenomenon was more profound in urban areas. In urban areas, 2D and 3D building morphology indexes contributed 42.5 % and 57.5 %, respectively, to vegetation greening trends. In rural areas, 2D building morphology indexes contributed 46.20 % to vegetation greening trends, while the relative contribution of 3D building morphology indexes to vegetation greening trends was 53.8 %.

Table 2
Overall vegetation changes trends in built-up environment.

Classification	Percentage (%)	Averaged Slope
Significant greening	11.89	0.0078
Significant browning	4.30	−0.0083
No change	0.16	0
Not significant greening	52.23	0.0034
Not significant browning	31.42	−0.0027

Table 3
Features of overall vegetation changes in urban and rural areas.

Greenness and its changes indexes	Urban	Rural
Averaged slope of greening	0.0035	0.005
Averaged slope of browning	−0.0031	−0.0037
Percentage of greening (%)	62.71	65.38
Percentage of browning (%)	37.22	34.60

Table 4
Correlation coefficients between vegetation greening and building morphology.

Correlation type	2D building morphology	Correlation coefficient	3D building morphology	Correlation coefficient
Pearson	BCR	−0.21 * *	BVD	−0.17 * *
	LPI	−0.16 * *	SVF	0.17 * *
	LSI	−0.17 * *	MBH	−0.13 * *
	ED	−0.20 * *	FAR	−0.17 * *
	Average absolute value of 2D metrics	0.19	Average absolute value of 3D metrics	0.16
Spearman	BCR	−0.18 * *	BVD	−0.17 * *
	LPI	−0.17 * *	SVF	0.15 * *
	LSI	−0.15 * *	MBH	−0.13 * *
	ED	−0.17 * *	FAR	−0.17 * *
	Average absolute value of 2D metrics	0.17	Average absolute value of 3D metrics	0.16

Note: * * the level of significance at 0.01.

4.3.2. The marginal effect of 2D/3D building morphology on vegetation greening trends

Given that correlation analyses might underestimate the relationship between 2D/3D building morphology and vegetation greening, we further utilized Boosted Regression Trees (BRT) to analyze the non-monotonic and nonlinear marginal effect of each building morphology on vegetation greening trends in urban (Fig. 5) and rural areas (Fig. 6). The marginal effects, according to the BRT model, demonstrate how changes in 2D/3D building morphology influence vegetation greening. The marginal effect of SVF, LPI, MBH, and ED on vegetation greening showed similar trends in urban and rural areas. The impact of SVF on vegetation greening changed from negative to positive at a threshold of 0.82 in urban areas and 0.88 in rural areas. This means that it is beneficial for vegetation greening when the visible sky occupies around 80 % of the entire hemispherical sky. LPI positively affected vegetation greening below 15 in urban areas and below 5 in rural areas, thereafter exerting a stable negative effect. MBH's effect on vegetation greening shifted from negative to slightly positive at thresholds of 35 m in urban areas and 12 m in rural areas. ED's impact on vegetation greening transitioned from positive to negative at thresholds of 0.037 m/m^2 in urban and 0.006 m/m^2 in rural areas. The marginal effects of BVD and LSI differed between urban and rural areas. In urban areas, BVD initially had a positive effect below 3, turned negative beyond that, and had no impact above 12. This means that when the volume density of buildings is less than 3 m^3/m^2, it would enhance the vegetation greening. While in rural areas, BVD presented a negative effect below 0.1 m^2/m^3 and became a positive effect until its value exceeded 1.3. Therefore, for rural areas, keeping BVD between 0.1 and 1.3 m^3/m^2 is optimal for enhancing vegetation growth. LSI's impact on vegetation greening in urban areas changed from a negative effect to a positive effect at the threshold of 2.2. In the rural areas, LSI's marginal effect on vegetation greening became positive at 1.05, peaked at 1.2, and turned negative above 3.65. LSI measures the complexity of buildings' shapes. A higher LSI value indicates that the building shapes are more irregular and complex. Therefore, a slight increase in the complexity and irregularity of

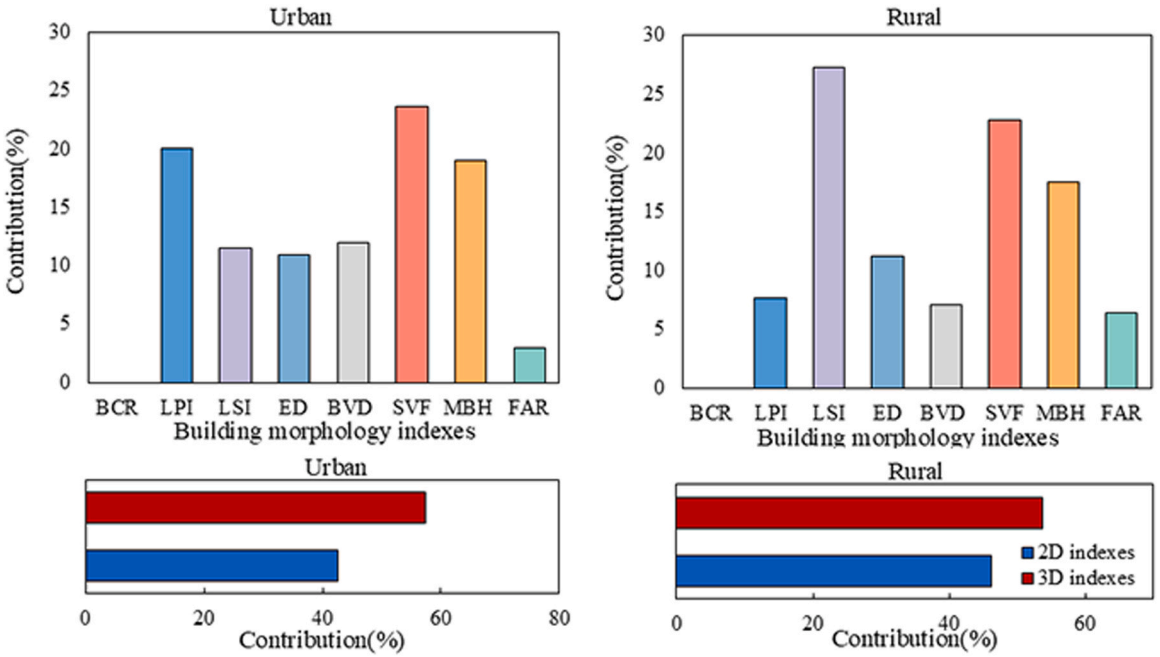

Fig. 4. Relative contributions (%) of 2D/3D building morphology to vegetation greening trends in urban and rural areas.

buildings is beneficial for vegetation greening (2.2–3.3 times more complex than a square in urban areas, and 1.05–3.65 times more complex than a square in rural areas), but too much complexity is not beneficial for vegetation greening (exceeds 3.3 times that of a square and exceeds 3.65 times that of a square). FAR and BCR have virtually no impact on vegetation greening both in urban and rural areas.

5. Discussion

5.1. The complexity of the building morphology - vegetation greening relationship

Unlike previous studies that have mostly explored the relationship between vegetation greening and CO_2 fertilization (Keenan et al., 2013; Ukkola et al., 2016), climate changes (Keenan and Riley, 2018; Nemani et al., 2003), land use changes (Shen et al., 2023), and nitrogen deposition (Greaver et al., 2016). Our study highlighted and confirmed the important role of 2D/3D building morphology for vegetation greening trends using the Pearson/ Spearman correlation method and BRT model. Although a low yet statistically significant correlation between 2D/3D building morphology and vegetation greening was identified, this suggests that building morphology is a significant but partial factor in greening, with other important determinants also playing roles. There are other important determinants as well. However, we still need to understand the impacts of 2D/3D building morphology on vegetation greening to foster a more comprehensive understanding of the influencing factors of vegetation greening.

Our results suggested that 3D building morphology indexes have a stronger impact on vegetation greening than 2D indexes. Cao et al. (2021) also demonstrated that 3D building morphology indexes crucially affect the urban climate environment more than 2D indexes. Consequently, it is crucial to prioritize the role of 3D building morphology in urban climate and vegetation greening studies and to develop more 3D morphology indexes for future research. Interestingly, despite previous studies suggesting an influence of BCR on vegetation greening, our results showed that BCR had virtually no impact on vegetation greening. Additionally, 3D building morphology indicators had a more significant impact on vegetation greening than 2D indicators (Fig. 4). We speculate that the greater impact of 3D indicators may be attributed to their inclusion in the regression model, which offers a more comprehensive reflection of building features and environments. These phenomena both illustrated the necessity of considering the impact of 3D building morphology on vegetation greening trends. Given the complexity of the built environment, future urban climate studies should develop more physically meaningful 3D building morphology measures.

Furthermore, we found that both Pearson and Spearman analyses may underestimate the relationship between 2D/3D building morphology and vegetation greening. The Pearson correlation analysis demonstrated a potential nonlinear relationship in Hong Kong, while Spearman correlation analysis indicated a potential non-monotonic relationship. BRT model results confirmed the nonlinearity and non-monotonic nature of this relationship, which indicated the impact of 2D/3D building morphology on vegetation greening is not a monotonous positive or negative relationship. Therefore, as an advanced machine learning model, BRT facilitates the detection of non-monotonic and nonlinear relationships, contributing to a more profound comprehension of the intricate interactions between 2D/3D building morphology and vegetation greening.

There exist some important thresholds in the relationship between building morphology and vegetation greening, such as the threshold for the conversion of positive and negative effects, and the threshold for the maximum positive and negative effects, which may help us better understand the complex effects of urban building on vegetation greening and green city planning. These thresholds vary across cities as the environmental impacts of building morphology are influenced by the local climate, geography, vegetation types, and human activities (Banerjee et al., 2022). For example, in humid climate conditions, vegetation may more easily adapt to high-density buildings, whereas in arid climate conditions, vegetation may rely more on open spaces and good air circulation. Therefore, it is imperative to develop a further understanding of the effects of building morphology on vegetation greening in different cities with various features. Additionally, the observed nonlinearities indicated the optimal threshold of building morphology indexes for maximum and efficient greening effect. Specifically, marginal effects results showed that the impacts of SVF and LSI on vegetation greening transitioned from negative to positive. This indicated that higher values of SVF and LSI were associated with increased greening in both urban and rural areas. The SVF quantifies the

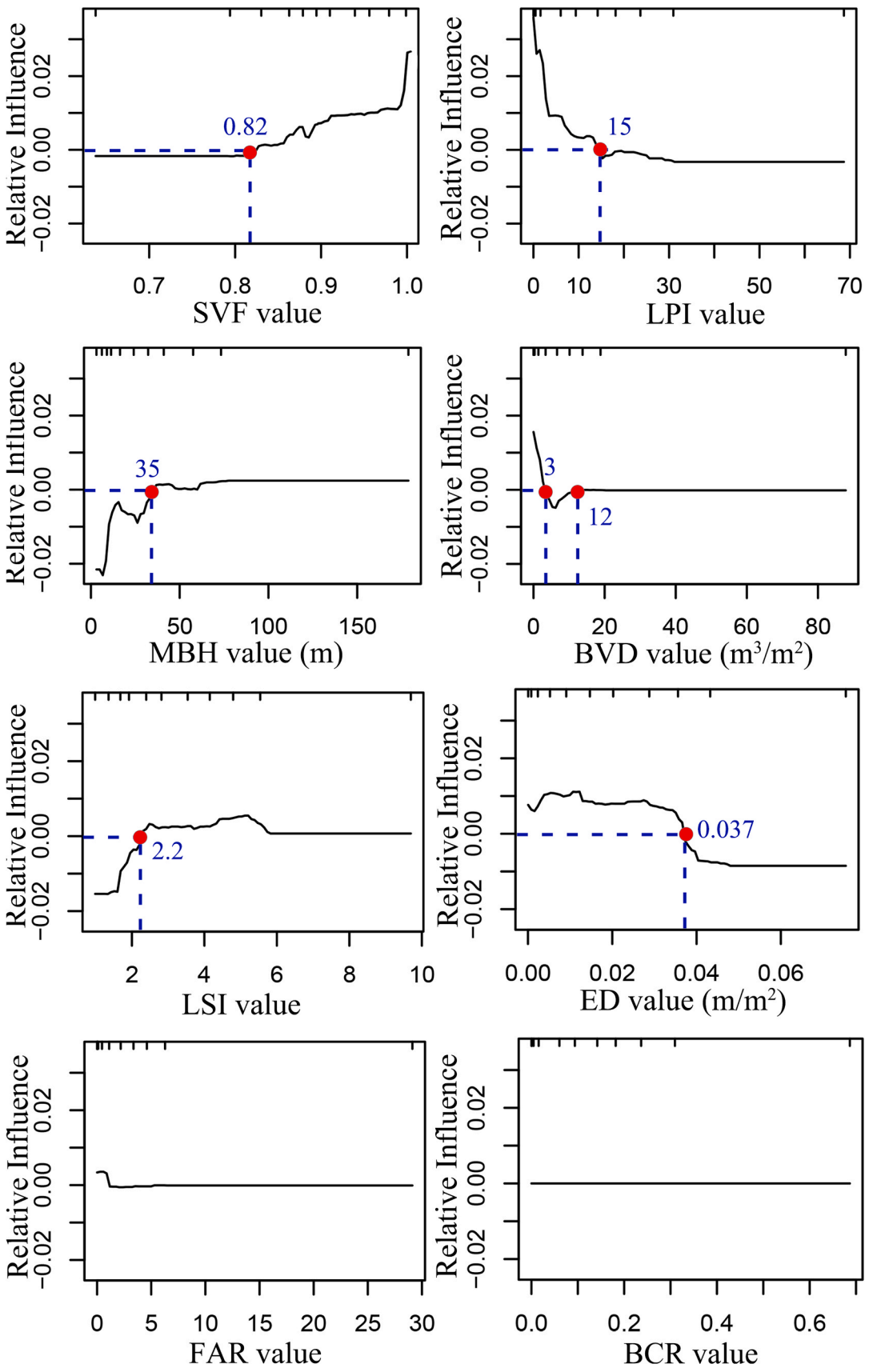

Fig. 5. The marginal effect of 2D/3D building morphology on vegetation greening in the urban areas of Hong Kong.

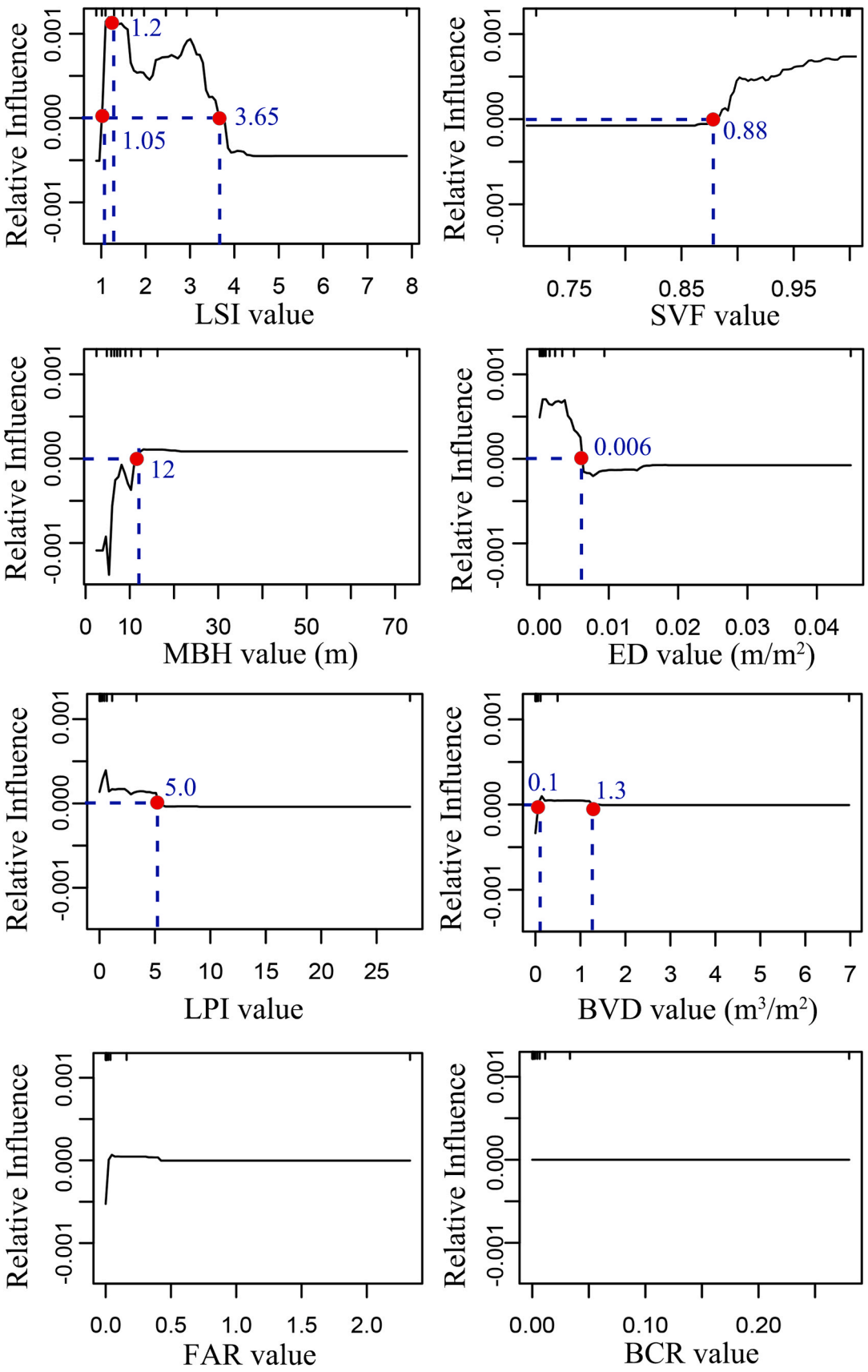

Fig. 6. The marginal effect of 2D/3D building morphology on vegetation greening in the rural areas of Hong Kong.

extent to which the sky at a certain point is obstructed by the surrounding environment. A higher SVF correlates with a more open environment, enhanced reception of solar radiation, and improved air circulation (Cao et al., 2021; Chatzipoulka et al., 2018). The more open the sky view, meaning the larger the proportion of visible sky relative to the entire hemispherical sky, the more it helps promote vegetation greening. The impacts of LPI and ED were characterized by a transition from positive effects to negative effects at certain thresholds (15 in urban areas and 5 in rural areas for LPI, 0.037 in urban areas and 0.006 in rural areas for ED). LPI, which measures the percentage of the largest building patch, indicates the degree of connectivity. The distribution of continuous and large-area buildings (LPI>15 in urban areas, LPI >5 in rural areas) was detrimental to vegetation greening. This may be because the larger buildings may reduce vegetation coverage and restrict air circulation, potentially impacting vegetation greening [62]. ED measures the ratio of the total length of edges in buildings, indicating the degree of fragmentation of buildings. An ED below 0.037 m/m^2 in urban areas and below 0.006 m/m^2 in rural areas enhanced vegetation greening, while higher fragmentation inhibited it. It is likely that higher ED leads to smaller, more isolated patches of green space and hinders the speed of vegetation greening processes.

5.2. Differences in urban and rural greening mechanism

Our study highlights significant differences in the urban-rural gradient of greening trends and their influencing factors. First, rural areas exhibited a higher degree of vegetation greening compared to urban regions (Table 4). These urban-rural differences could lead to disparities in ecosystem services provided by vegetation, exacerbating climate and ecological risks in urban areas, such as heat hazards, drought risks, and pollution hazards (Coleman et al., 2021; Cueva et al., 2022; Li et al., 2024). Therefore, understanding and identifying the determinants behind these urban-rural differences in vegetation greening is crucial for mitigating climate and ecological issues amid rapid urbanization. Second, significant differences were observed in the impacts of 2D/3D building morphology on vegetation greening between urban and rural areas. In urban areas, SVF was the predominant factor, while LSI was more influential in rural areas. This finding underscores the importance of analyzing urban-rural differences. Urban-rural differences were further evident in the marginal effects of 2D/3D building morphology on vegetation greening. Specifically, the turning points for each 2D/3D building morphology index varied across urban and rural areas, which can inform the building morphology optimization for both urban and rural areas. Additionally, LSI showed opposing influence patterns in urban versus rural areas. These phenomena both underline the different influencing factors and characteristics for vegetation greening in urban and rural areas, meriting further attention. These findings provide practical insights for building morphology planning in sustainable development and emphasize the need for differentiated management and planning in urban and rural areas.

5.3. Policy implications

Understanding the impacts of 2D/3D building morphology on vegetation greening is instrumental for the development of green, resilient, sustainable cities, and contributes to the Sustainable Development Goal (SDG) 11. This study demonstratesd that 2D/3D building morphology significantly influences vegetation greening in Hong Kong. Our findings deepen understanding of how building morphology characteristics impact urban environments. Additionally, our results offer actionable insights for optimizing building morphology to enhance urban greening and renewal, especially in high-density areas like Hong Kong.

In the process of designing green cities, planners and policymakers can achieve a greener environment by optimizing building layouts in both horizontal and vertical dimensions. The relative contributions and the nonlinear relationships with turning points in 2D/3D building morphology, as revealed by the BRT model, provide crucial data to guide policy and planning. Urban-rural differences identified in this study support targeted and differentiated building layout optimization, advancing sustainable development. Rural areas, often reserved for future urban expansion, can benefit from our urban findings to guide their development strategies. Specifically, for urban areas, given that the SVF is crucial, optimal SVF design through strategic building layouts is essential to meet regional development needs. For example, maintaining the SVF above 0.82, as recommended by the marginal effect curve, can effectively promote vegetation greening. In rural areas, LSI between 1.05 and 3.65 maximizes its positive impact on greening, especially at an LSI of 1.2.

5.4. Limitations and future research directions

This study has several limitations that warrant further discussion. First, according to the record of Hong Kong Herbarium, the vegetation types/species are greater than 3300 in Hong Kong. Responses of vegetation greening to 2D/3D building morphology may vary among different vegetation types. Due to the lack of high-resolution data on vegetation types in Hong Kong, this study failed to consider the potential impact of vegetation types on the relationship between vegetation greening and 2D/3D building morphology. Second, due to the lack of multi-temporal and high-resolution building height data, this study only focused on Hong Kong, which restricts the generalizability of this research. To thoroughly investigate these issues, it is essential to obtain high-resolution building height data that encompasses long-term changes and extensive spatial coverage. Third, this study has chosen the EVI as the representative of vegetation greenness because of its robust performance and widespread use in vegetation trend monitoring (Fan et al., 2023; Zhou et al., 2023). However, there are plentiful other indices that can also characterize vegetation conditions, such as the Normalized Difference Vegetation Index (NDVI), Net Primary Production (NPP), Gross Primary Productivity (GPP), and even the newly developed kernel NDVI (kNDVI) (Camps-Valls et al., 2021; Wang et al., 2020; Yuan et al., 2007). These indices provide different perspectives and have shown inconsistencies in various studies (Ding et al., 2020; Zhou et al., 2023). Therefore, future research should incorporate multiple indices to thoroughly study the impact of building morphology on vegetation characteristics. Fourth, the analysis in this study was conducted at the pixel level with a resolution of 250 m. Our regression method does not allow for the detection of spatial interactions between adjacent pixels. Incorporating spatial econometric models into future research could be valuable. Additionally, previous studies have documented scale-dependent effects in geographical and ecological processes (Chisholm et al., 2013; Wu, 2004). Incorporating multi-scale analysis, such as using pixels of varying resolutions and community-scale assessments, would help interpret scale effects. Fifth, we relied solely on GUB data to differentiate between urban and rural areas. Although GUB data can effectively separate urban and rural areas based on artificial impervious surfaces. However, definitions of urban and rural areas can vary based on different criteria, such as population, gross domestic product, and nighttime light (Florczyk et al., 2019; Li and Zhou, 2017). Using different datasets could introduce variations in the results. Therefore, evaluating and employing suitable multimodal datasets to analyze urban-rural differences is a recommended future direction. Finally, while our study preliminarily demonstrated the nonlinear relationship between 2D/3D building morphology and vegetation greening, understanding the underlying mechanisms remains complex. More evidence from field measurements and microclimate simulations is needed to further explore these mechanisms.

6. Conclusions

This study developed an analytical framework that employs

Pearson/Spearman correlation analysis and the Boosted Regression Trees (BRT) model to explore the relationship between 2D/3D building morphology and vegetation greening in Hong Kong. Our analysis revealed that from 2010 to 2020, approximately 69.10 % of Hong Kong exhibited a prevalent vegetation greening trend, quantified by a slope of 0.0024. We observed significant disparities in greening trends between urban and rural areas. The correlation between 2D/3D building morphology and vegetation greening was found to be low yet statistically significant. 3D building morphology had more pronounced effects on vegetation greening compared to 2D. Furthermore, the influences of 2D/3D building morphology on vegetation greening demonstrated significant urban-rural differences and exhibited high nonlinearity. SVF had the largest impact in urban areas, while LSI was most influential in rural areas. The impact patterns of SVF, MBH, LPI, and ED on greening were similar across urban and rural areas, but the turning points where the effects shifted between positive and negative were different. SVF and MBH effects shifted from negative to positive effects, while LPI and ED shifted from positive to negative effects. In rural areas, LSI's impact shifted from negative to positive, while in urban areas, it changed from negative to positive and back to negative effect. BVD exhibited a shift from positive to negative effects in urban areas and from negative to positive effects in rural areas. This study expands the understanding of the complicated and nonlinear relationship between 2D/3D building morphology and vegetation greening in both urban and rural areas, offering valuable insights for future research and the optimization of building morphology in pursuit of sustainable urban development.

Author statement

This paper is an original work and is not currently being considered for publication, in part or in whole, by any other journal.

CRediT authorship contribution statement

Qihao Weng: Writing – review & editing, Supervision, Resources, Project administration, Funding acquisition, Conceptualization. **Yu Liu:** Writing – review & editing, Writing – original draft, Visualization, Software, Methodology, Investigation, Formal analysis, Conceptualization.

Declaration of Competing Interest

The authors declare no conflict of interest.

Acknowledgments

This research has received funding from Global STEM Professorship, Hong Kong SAR Government (P0039329), Hong Kong RGC GRF (15300923), and Hong Kong Polytechnic University (P0046482, P0038446, and P0042484). We also thank Dr. Qiming Zheng and Dr. Siqi Jia for their help in drafting the manuscript.

Appendix

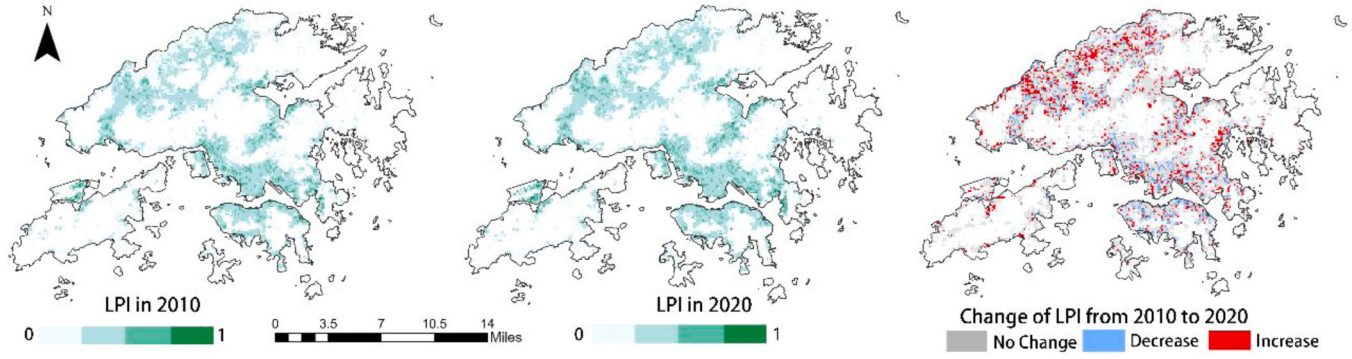

Figure A1. Spatial distribution of the largest patch index (LPI) and changes from 2010 to 2020.

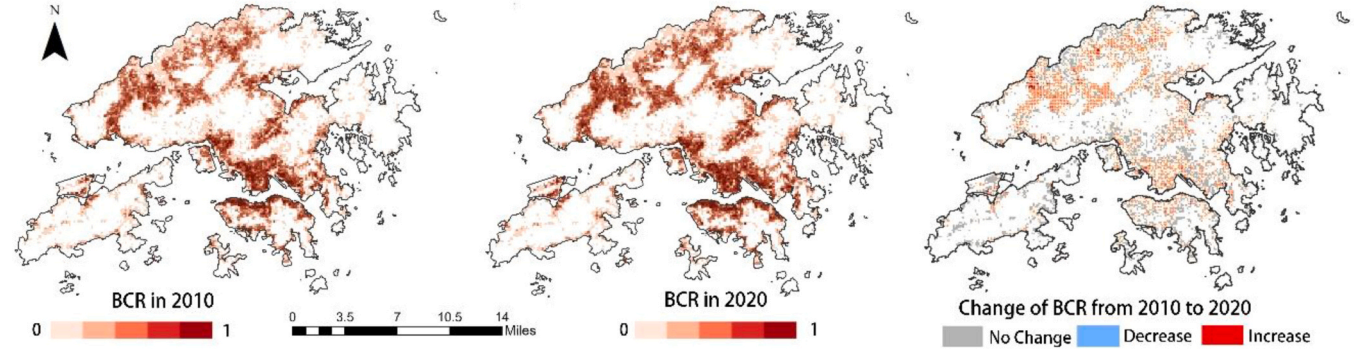

Figure A2. Spatial distribution of the building coverage ratio (BCR) and changes from 2010 to 2020.

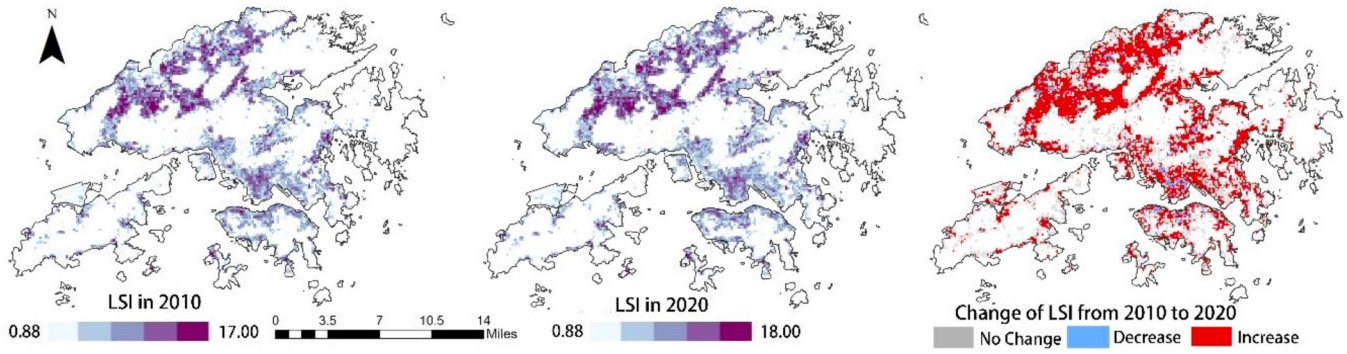

Figure A3. Spatial distribution of the landscape shape index (LSI) and changes from 2010 to 2020.

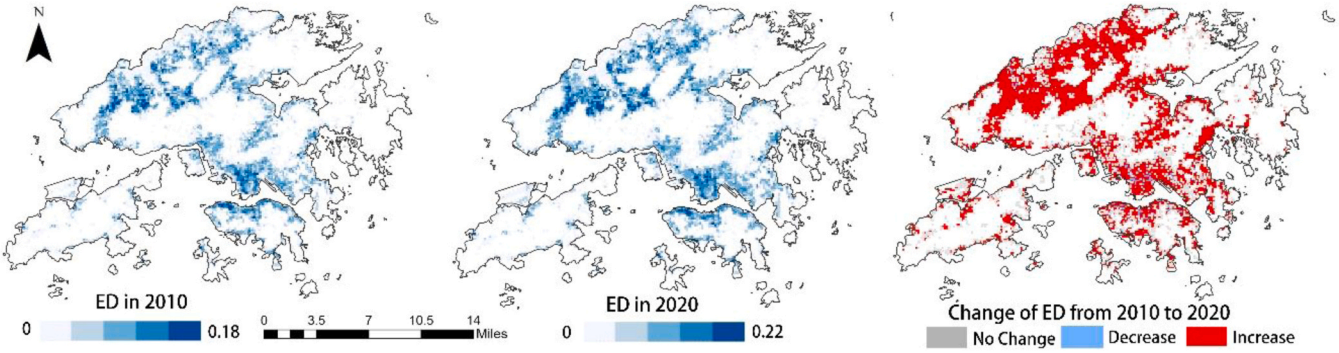

Figure A4. Spatial distribution of the edge density (ED) and changes from 2010 to 2020.

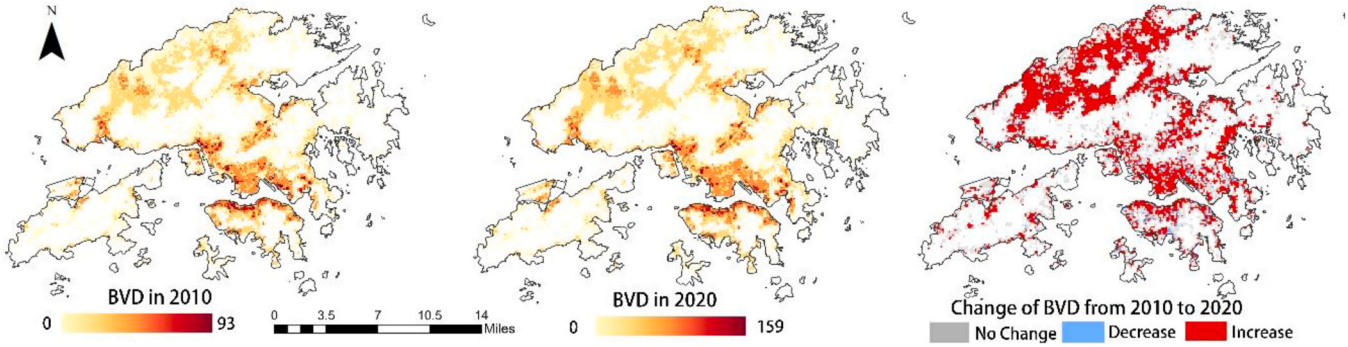

Figure A5. Spatial distribution of the building volume density (BVD) and changes from 2010 to 2020.

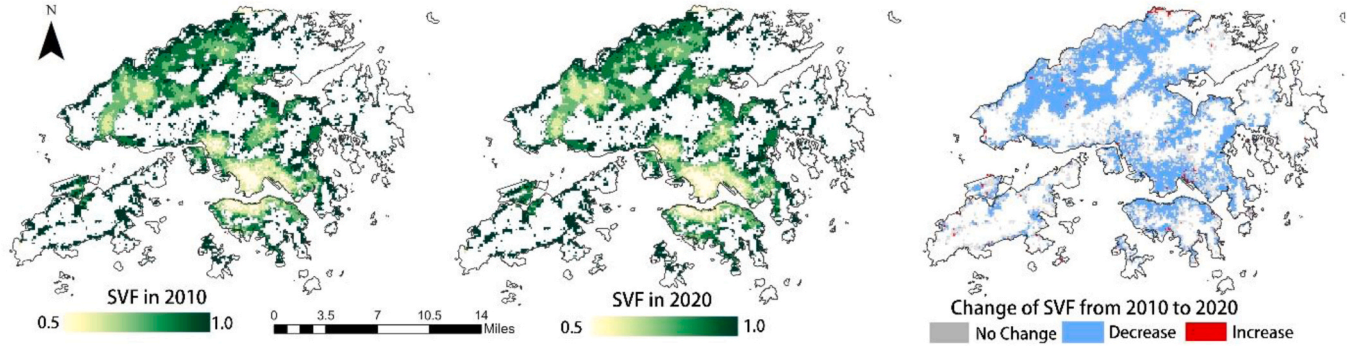

Figure A6. Spatial distribution of the sky view factor (SVF) and changes from 2010 to 2020.

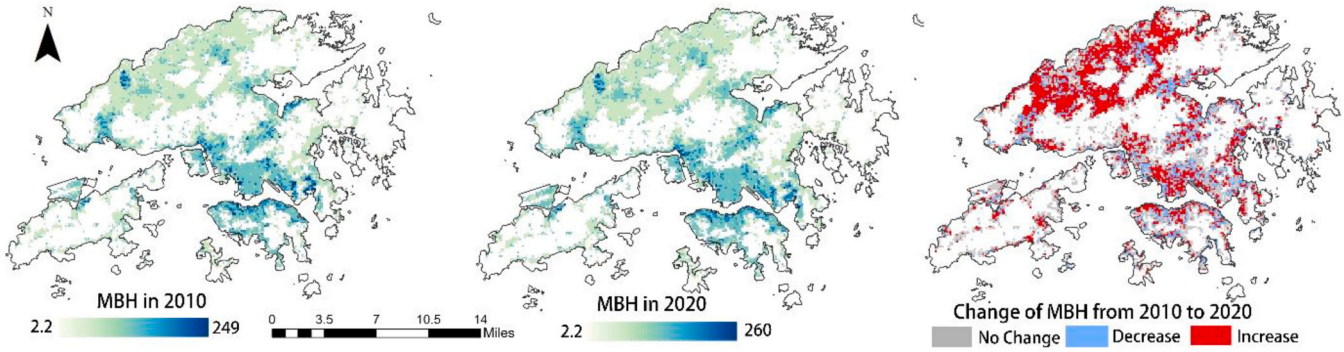

Figure A7. Spatial distribution of the mean building height (MBH) and changes from 2010 to 2020.

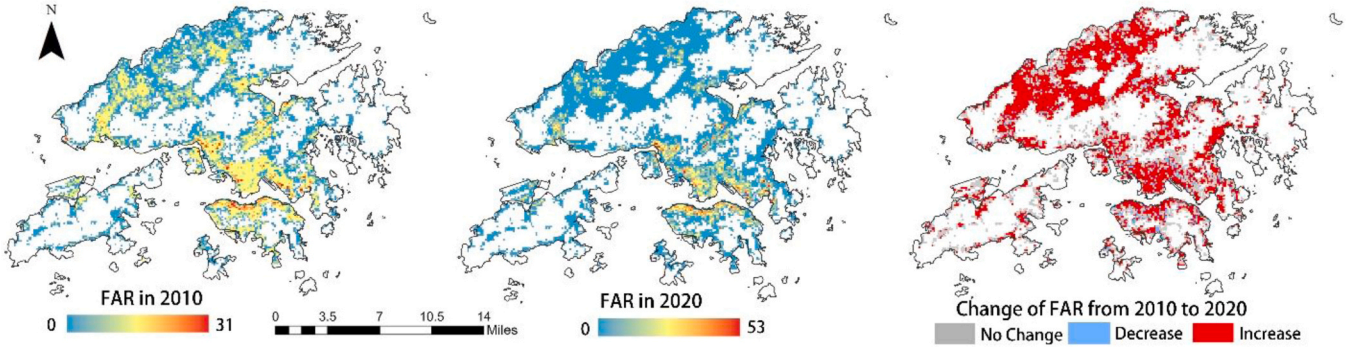

Figure A8. Spatial distribution of the floor area ratio (FAR) and changes from 2010 to 2020.

References

Alexander, C., 2021. Influence of the proportion, height and proximity of vegetation and buildings on urban land surface temperature. Int. J. Appl. Earth Obs. Geoinf. 95, 102265.

Allen-Dumas, M.R., Rose, A.N., New, J.R., Omitaomu, O.A., Yuan, J., Branstetter, M.L., Sylvester, L.M., Seals, M.B., Carvalhaes, T.M., Adams, M.B., Bhandari, M.S., Shrestha, S.S., Sanyal, J., Berres, A.S., Kolosna, C.P., Fu, K.S., Kahl, A.C., 2020. Impacts of the morphology of new neighborhoods on microclimate and building energy. Renew. Sustain. Energy Rev. 133, 110030. https://doi.org/10.1016/j.rser.2020.110030.

Azhdari, A., Soltani, A., Alidadi, M., 2018. Urban morphology and landscape structure effect on land surface temperature: evidence from Shiraz, a semi-arid city. Sustain. Cities Soc. 41, 853–864.

Ballantyne, A., Smith, W., Anderegg, W., Kauppi, P., Sarmiento, J., Tans, P., Shevliakova, E., Pan, Y., Poulter, B., Anav, A., Friedlingstein, P., Houghton, R., Running, S., 2017. Accelerating net terrestrial carbon uptake during the warming hiatus due to reduced respiration. Nat. Clim. Change 7, 148–152. https://doi.org/10.1038/nclimate3204.

Banerjee, S., Ching, N.Y., G, Yik, S.K., Dzyuban, Y., Crank, P.J., Pek Xin Yi, R., Chow, W. T.L., 2022. Analysing impacts of urban morphological variables and density on outdoor microclimate for tropical cities: a review and a framework proposal for future research directions. Build. Environ. 225, 109646. https://doi.org/10.1016/j.buildenv.2022.109646.

Baniya, B., Tang, Q., Pokhrel, Y., Xu, X., 2019. Vegetation dynamics and ecosystem service values changes at national and provincial scales in Nepal from 2000 to 2017. Environ. Dev. 32, 100464.

Camps-Valls, G., Campos-Taberner, M., Moreno-Martínez, Á., Walther, S., Duveiller, G., Cescatti, A., Mahecha, M.D., Muñoz-Marí, J., García-Haro, F.J., Guanter, L., 2021. A unified vegetation index for quantifying the terrestrial biosphere. Sci. Adv. 7, eabc7447.

Cao, Q., Luan, Q., Liu, Y., Wang, R., 2021. The effects of 2D and 3D building morphology on urban environments: a multi-scale analysis in the Beijing metropolitan region. Build. Environ. 192, 107635. https://doi.org/10.1016/j.buildenv.2021.107635.

Chang, Q., Xiao, X., Doughty, R., Wu, X., Jiao, W., Qin, Y., 2021. Assessing variability of optimum air temperature for photosynthesis across site-years, sites and biomes and their effects on photosynthesis estimation. Agric. For. Meteorol. 298–299, 108277. https://doi.org/10.1016/j.agrformet.2020.108277.

Chatzipoulka, C., Compagnon, R., Kaempf, J., Nikolopoulou, M., 2018. Sky view factor as predictor of solar availability on building façades. Sol. Energy 170, 1026–1038. https://doi.org/10.1016/j.solener.2018.06.028.

Chen, C., Bagan, H., Yoshida, T., Borjigin, H., Gao, J., 2022. Quantitative analysis of the building-level relationship between building form and land surface temperature using airborne LiDAR and thermal infrared data. Urban Clim. 45, 101248.

Chisholm, R.A., Muller-Landau, H.C., Abdul Rahman, K., Bebber, D.P., Bin, Y., Bohlman, S.A., Bourg, N.A., Brinks, J., Bunyavejchewin, S., Butt, N., 2013. Scale-dependent relationships between tree species richness and ecosystem function in forests. J. Ecol. 101, 1214–1224.

Coleman, C.J., Yeager, R.A., Riggs, D.W., Coleman, N.C., Garcia, G.R., Bhatnagar, A., Pope, C.A., 2021. Greenness, air pollution, and mortality risk: A U.S. cohort study of cancer patients and survivors. Environ. Int. 157, 106797. https://doi.org/10.1016/j.envint.2021.106797.

Cueva, J., Yakouchenkova, I.A., Fröhlich, K., Dermann, A.F., Dermann, F., Köhler, M., Grossmann, J., Meier, W., Bauhus, J., Schröder, D., Sardemann, G., Thomas, C., Carnicero, A.R., Saha, S., 2022. Synergies and trade-offs in ecosystem services from urban and peri-urban forests and their implication to sustainable city design and planning. Sustain. Cities Soc. 82, 103903. https://doi.org/10.1016/j.scs.2022.103903.

Daramola, M.T., Balogun, I.A., 2019. Analysis of the urban surface thermal condition based on sky-view factor and vegetation cover. Remote Sens. Appl. Soc. Environ. 15, 100253.

De'ath, G., 2007. Boosted trees for ecological modeling and prediction. Ecology 88, 243–251. https://doi.org/10.1890/0012-9658(2007)88[243:BTFEMA]2.0.CO;2.

Ding, Z., Peng, J., Qiu, S., Zhao, Y., 2020. Nearly half of global vegetated area experienced inconsistent vegetation growth in terms of greenness, cover, and productivity. Earth Future 8, e2020EF001618.

Fan, F., Xiao, C., Feng, Z., Yang, Y., 2023. Impact of human and climate factors on vegetation changes in mainland southeast asia and yunnan province of China. J. Clean. Prod. 415, 137690. https://doi.org/10.1016/j.jclepro.2023.137690.

Florczyk, A., Melchiorri, M., Corbane, C., Schiavina, M., Pesaresi, M., Panagiotis, P., Sabo, F., Freire, S., Ehrlich, D., Kemper, T., Tommasi, P., Airaghi, D., Zanchetta, L., 2019. Description of the GHS Urban Centre Database 2015. https://doi.org/10.2760/037310.

Gong, P., Li, X., Wang, J., Bai, Y., Chen, B., Hu, T., Liu, X., Xu, B., Yang, J., Zhang, W., 2020. Annual maps of global artificial impervious area (GAIA) between 1985 and 2018. Remote Sens. Environ. 236, 111510.

Greaver, T.L., Clark, C.M., Compton, J.E., Vallano, D., Talhelm, A.F., Weaver, C.P., Band, L.E., Baron, J.S., Davidson, E.A., Tague, C.L., 2016. Key ecological responses to nitrogen are altered by climate change. Nat. Clim. Change 6, 836–843.

Haberl, H., Erb, K.H., Krausmann, F., Gaube, V., Bondeau, A., Plutzar, C., Gingrich, S., Lucht, W., Fischer-Kowalski, M., 2007. Quantifying and mapping the human

appropriation of net primary production in earth's terrestrial ecosystems. Proc. Natl. Acad. Sci. U. S. A. 104, 12942–12947. https://doi.org/10.1073/pnas.0704243104.
Han, D., An, H., Wang, F., Xu, X., Qiao, Z., Wang, M., Sui, X., Liang, S., Hou, X., Cai, H., 2022. Understanding seasonal contributions of urban morphology to thermal environment based on boosted regression tree approach. Build. Environ. 226, 109770.
Han, S., Hou, H., Estoque, R.C., Zheng, Y., Shen, C., Murayama, Y., Pan, J., Wang, B., Hu, T., 2023. Seasonal effects of urban morphology on land surface temperature in a three-dimensional perspective: a case study in Hangzhou, China. Build. Environ. 228, 109913. https://doi.org/10.1016/j.buildenv.2022.109913.
He, Y., Liu, Z., Ng, E., 2022. Parametrization of irregularity of urban morphologies for designing better pedestrian wind environment in high-density cities – a wind tunnel study. Build. Environ. 226, 109692. https://doi.org/10.1016/j.buildenv.2022.109692.
Hu, Y., Dai, Z., Guldmann, J.-M., 2020. Modeling the impact of 2D/3D urban indicators on the urban heat island over different seasons: a boosted regression tree approach. J. Environ. Manag. 266, 110424. https://doi.org/10.1016/j.jenvman.2020.110424.
Huete, A., Didan, K., Miura, T., Rodriguez, E.P., Gao, X., Ferreira, L.G., 2002. Overview of the radiometric and biophysical performance of the MODIS vegetation indices. Remote Sens. Environ. 83, 195–213.
Ji, Y., Zhan, W., Du, H., Wang, S., Li, L., Xiao, J., Liu, Z., Huang, F., Jin, J., 2023. Urban-rural gradient in vegetation phenology changes of over 1500 cities across China jointly regulated by urbanization and climate change. ISPRS J. Photogramm. Remote Sens. 205, 367–384. https://doi.org/10.1016/j.isprsjprs.2023.10.015.
Jia, W., Zhao, S., Zhang, X., Liu, S., Henebry, G.M., Liu, L., 2021. Urbanization imprint on land surface phenology: the urban–rural gradient analysis for Chinese cities. Glob. Change Biol. 27, 2895–2904. https://doi.org/10.1111/gcb.15602.
Kamal, A., Abidi, S.M.H., Mahfouz, A., Kadam, S., Rahman, A., Hassan, I.G., Wang, L.L., 2021. Impact of urban morphology on urban microclimate and building energy loads. Energy Build. 253, 111499. https://doi.org/10.1016/j.enbuild.2021.111499.
Keenan, T.F., Hollinger, D.Y., Bohrer, G., Dragoni, D., Munger, J.W., Schmid, H.P., Richardson, A.D., 2013. Increase in forest water-use efficiency as atmospheric carbon dioxide concentrations rise. Nature 499, 324–327.
Keenan, T.F., Riley, W.J., 2018. Greening of the land surface in the world's cold regions consistent with recent warming. Nat. Clim. Change 8, 825–828.
Li, X., Gong, P., Zhou, Y., Wang, J., Bai, Y., Chen, B., Hu, T., Xiao, Y., Xu, B., Yang, J., Liu, X., Cai, W., Huang, H., Wu, T., Wang, X., Lin, P., Li, Xun, Chen, J., He, C., Li, Xia, Yu, L., Clinton, N., Zhu, Z., 2020. Mapping global urban boundaries from the global artificial impervious area (GAIA) data. Environ. Res. Lett. 15, 094044. https://doi.org/10.1088/1748-9326/ab9be3.
Li, Z., Hu, D., 2022. Exploring the relationship between the 2D/3D architectural morphology and urban land surface temperature based on a boosted regression tree: a case study of Beijing, China. Sustain. Cities Soc. 78, 103392. https://doi.org/10.1016/j.scs.2021.103392.
Li, Z., Sun, F., Wang, H., Wang, T., Feng, Y., 2024. Detecting the interactions between vegetation greenness and drought globally. Atmos. Res. 304, 107409. https://doi.org/10.1016/j.atmosres.2024.107409.
Li, X., Wang, K., Huntingford, C., Zhu, Z., Peñuelas, J., Myneni, R.B., Piao, S., 2024. Vegetation greenness in 2023. Nat. Rev. Earth Environ. https://doi.org/10.1038/s43017-024-00543-z.
Li, H., Wu, J., 2004. Use and misuse of landscape indices. Landsc. Ecol. 19, 389–399.
Li, D., Wu, S., Liang, Z., Li, S., 2020. The impacts of urbanization and climate change on urban vegetation dynamics in China. Urban For. Urban Green. 54, 126764. https://doi.org/10.1016/j.ufug.2020.126764.
Li, L., Zhan, W., Ju, W., Peñuelas, J., Zhu, Z., Peng, S., Zhu, X., Liu, Z., Zhou, Y., Li, J., Lai, J., Huang, F., Yin, G., Fu, Y., Li, M., Yu, C., 2023. Competition between biogeochemical drivers and land-cover changes determines urban greening or browning. Remote Sens. Environ. 287, 113481. https://doi.org/10.1016/j.rse.2023.113481.
Li, N., Zhao, F., Chen, S., Li, C., Wang, Y., Ma, Y., Chen, L., 2024. Indirect non-linear effects of landscape patterns on vegetation growth in Kunming City. npj Urban Sustain 4, 30. https://doi.org/10.1038/s42949-024-00165-w.
Li, X., Zhou, W., Ouyang, Z., Xu, W., Zheng, H., 2012. Spatial pattern of greenspace affects land surface temperature: evidence from the heavily urbanized Beijing metropolitan area, China. Landsc. Ecol. 27, 887–898.
Li, X., Zhou, Y., 2017. Urban mapping using DMSP/OLS stable night-time light: a review. Int. J. Remote Sens. 38, 6030–6046. https://doi.org/10.1080/01431161.2016.1274451.
Liu, M., Hu, Y.-M., Li, C.-L., 2017. Landscape metrics for three-dimensional urban building pattern recognition. Appl. Geogr. 87, 66–72.
Liu, Z., Zhou, Y., Feng, Z., 2023. Response of vegetation phenology to urbanization in urban agglomeration areas: A dynamic urban–rural gradient perspective. Sci. Total Environ. 864, 161109. https://doi.org/10.1016/j.scitotenv.2022.161109.
Myneni, R.B., Keeling, C.D., Tucker, C.J., Asrar, G., Nemani, R.R., 1997. Increased plant growth in the northern high latitudes from 1981 to 1991. Nature 386, 698–702. https://doi.org/10.1038/386698a0.
Nemani, R.R., Keeling, C.D., Hashimoto, H., Jolly, W.M., Piper, S.C., Tucker, C.J., Myneni, R.B., Running, S.W., 2003. Climate-driven increases in global terrestrial net primary production from 1982 to 1999. science 300, 1560–1563.
Pan, N., Feng, X., Fu, B., Wang, S., Ji, F., Pan, S., 2018. Increasing global vegetation browning hidden in overall vegetation greening: Insights from time-varying trends. Remote Sens. Environ. 214, 59–72. https://doi.org/10.1016/j.rse.2018.05.018.
Pearson, K., 1908. On a mathematical theory of determinantal inheritance, from suggestions and notes of the late WFR Weldon. Biometrika 6, 80–93.
Pouteau, R., Rambal, S., Ratte, J.-P., Gogé, F., Joffre, R., Winkel, T., 2011. Downscaling MODIS-derived maps using GIS and boosted regression trees: the case of frost occurrence over the arid Andean highlands of Bolivia. Remote Sens. Environ. 115, 117–129. https://doi.org/10.1016/j.rse.2010.08.011.
Rawson, H.M., Begg, J.E., Woodward, R.G., 1977. The effect of atmospheric humidity on photosynthesis, transpiration and water use efficiency of leaves of several plant species. Planta 134, 5–10. https://doi.org/10.1007/BF00390086.
Rhee, J., Park, S., Lu, Z., 2014. Relationship between land cover patterns and surface temperature in urban areas. GIScience Remote Sens. 51, 521–536. https://doi.org/10.1080/15481603.2014.964455.
Ru, J., Zhou, Y., Hui, D., Zheng, M., Wan, S., 2018. Shifts of growing-season precipitation peaks decrease soil respiration in a semiarid grassland. Glob. Change Biol. 24, 1001–1011. https://doi.org/10.1111/gcb.13941.
Salvati, A., Monti, P., Roura, H.C., Cecere, C., 2019. Climatic performance of urban textures: Analysis tools for a Mediterranean urban context. Energy Build. 185, 162–179.
Serbin, S.P., Singh, A., Desai, A.R., Dubois, S.G., Jablonski, A.D., Kingdon, C.C., Kruger, E.L., Townsend, P.A., 2015. Remotely estimating photosynthetic capacity, and its response to temperature, in vegetation canopies using imaging spectroscopy. Remote Sens. Environ. Spec. Issue Hyperspectral Infrared Image (HyspIRI) 167, 78–87. https://doi.org/10.1016/j.rse.2015.05.024.
Shen, F., Yang, L., Zhang, L., Guo, M., Huang, H., Zhou, C., 2023. Quantifying the direct effects of long-term dynamic land use intensity on vegetation change and its interacted effects with economic development and climate change in jiangsu, China. J. Environ. Manag. 325, 116562.
Spearman, C., 1987. The proof and measurement of association between two things. Am. J. Psychol. 100, 441–471. https://doi.org/10.2307/1422689.
Tan, P.Y., Ismail, M.R.B., 2015. The effects of urban forms on photosynthetically active radiation and urban greenery in a compact city. Urban Ecosyst. 18, 937–961. https://doi.org/10.1007/s11252-015-0461-9.
Ukkola, A.M., Prentice, I.C., Keenan, T.F., Van Dijk, A.I., Viney, N.R., Myneni, R.B., Bi, J., 2016. Reduced streamflow in water-stressed climates consistent with CO2 effects on vegetation. Nat. Clim. Change 6, 75–78.
Wang, R., Gamon, J.A., Emmerton, C.A., Springer, K.R., Yu, R., Hmimina, G., 2020. Detecting intra-and inter-annual variability in gross primary productivity of a North American grassland using MODIS MAIAC data. Agric. For. Meteorol. 281, 107859.
Wang, X., Li, B., Liu, Y., Yang, Y., Fu, X., Shen, R., Xu, W., Yao, L., 2024. Trends and attributions of the long-term thermal comfort across the urban–rural gradient in major Chinese cities. Appl. Geogr. 164, 103221. https://doi.org/10.1016/j.apgeog.2024.103221.
Wang, Q., Peng, L.L.H., Jiang, W., Yin, S., Feng, N., Yao, L., 2024. Urban form affects the cool island effect of urban greenery via building shadows. Build. Environ. 254, 111398. https://doi.org/10.1016/j.buildenv.2024.111398.
Wu, J., 2004. Effects of changing scale on landscape pattern analysis: scaling relations. Landsc. Ecol. 19, 125–138.
Yang, C., Kui, T., Zhou, W., Fan, J., Pan, L., Wu, W., Liu, M., 2023. Impact of refined 2D/3D urban morphology on hourly air temperature across different spatial scales in a snow climate city. Urban Clim. 47, 101404.
Yao, L., 2024. Assessment of long time-series greening signatures across the urban–rural gradient in Chinese cities. Ecol. Indic. 160, 111826.
Yuan, W., Liu, S., Zhou, Guangsheng, Zhou, Guoyi, Tieszen, L.L., Baldocchi, D., Bernhofer, C., Gholz, H., Goldstein, A.H., Goulden, M.L., 2007. Deriving a light use efficiency model from eddy covariance flux data for predicting daily gross primary production across biomes. Agric. For. Meteorol. 143, 189–207.
Yuan, B., Zhou, L., Dang, X., Sun, D., Hu, F., Mu, H., 2021. Separate and combined effects of 3D building features and urban green space on land surface temperature. J. Environ. Manag. 295, 113116.
Zahid Iqbal, Q.M., Chan, A.L.S., 2016. Pedestrian level wind environment assessment around group of high-rise cross-shaped buildings: effect of building shape, separation and orientation. Build. Environ. 101, 45–63. https://doi.org/10.1016/j.buildenv.2016.02.015.
Zeng, Z., Piao, S., Li, L.Z., Zhou, L., Ciais, P., Wang, T., Li, Y., Lian, X.U., Wood, E.F., Friedlingstein, P., 2017. Climate mitigation from vegetation biophysical feedbacks during the past three decades. Nat. Clim. Change 7, 432–436.
Zeng, P., Sun, F., Liu, Y., Tian, T., Wu, J., Dong, Q., Peng, S., Che, Y., 2022. The influence of the landscape pattern on the urban land surface temperature varies with the ratio of land components: Insights from 2D/3D building/vegetation metrics. Sustain. Cities Soc. 78, 103599.
Zhang, J., Li, Z., Wei, Y., Hu, D., 2022. The impact of the building morphology on microclimate and thermal comfort-a case study in Beijing. Build. Environ. 223, 109469.
Zhang, L., Yang, L., Zohner, C.M., Crowther, T.W., Li, M., Shen, F., Guo, M., Qin, J., Yao, L., Zhou, C., 2022. Direct and indirect impacts of urbanization on vegetation growth across the world's cities. Sci. Adv. 8, eabo0095. https://doi.org/10.1126/sciadv.abo0095.
Zhao, S., Liu, S., Zhou, D., 2016. Prevalent vegetation growth enhancement in urban environment. Proc. Natl. Acad. Sci. U. S. A. 113, 6313–6318. https://doi.org/10.1073/pnas.1602312113.
Zhou, W., Huang, G., Cadenasso, M.L., 2011. Does spatial configuration matter? Understanding the effects of land cover pattern on land surface temperature in urban landscapes. Landsc. Urban Plan. 102, 54–63.

Zhou, W., Yu, W., Yao, Y., Jing, C., 2023. Understanding the indirect impacts of urbanization on vegetation growth using the Continuum of Urbanity framework. Sci. Total Environ. 899, 165693.
Zhou, D., Zhang, L., Hao, L., Sun, G., Xiao, J., Li, X., 2023. Large discrepancies among remote sensing indices for characterizing vegetation growth dynamics in Nepal. Agric. For. Meteorol. 339, 109546.
Zhu, Z., Piao, S., Myneni, R.B., Huang, M., Zeng, Z., Canadell, J.G., Ciais, P., Sitch, S., Friedlingstein, P., Arneth, A., Cao, C., Cheng, L., Kato, E., Koven, C., Li, Y., Lian, X., Liu, Y., Liu, R., Mao, J., Pan, Y., Peng, S., Peñuelas, J., Poulter, B., Pugh, T.A.M., Stocker, B.D., Viovy, N., Wang, X., Wang, Y., Xiao, Z., Yang, H., Zaehle, S., Zeng, N., 2016. Greening of the Earth and its drivers. Nat. Clim. Change 6, 791–795. https://doi.org/10.1038/nclimate3004.